INTERNATIONAL JOURNAL OF COMPUTERS COMMUNICATIONS & CONTROL
Online ISSN 1841-9844, ISSN-L 1841-9836, Volume: 20, Issue: 3, Month: June, Year: 2025
Article Number: 6919, https://doi.org/10.15837/ijccc.2025.3.6919

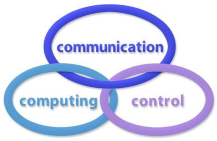

CCC Publications

Early detection of current faults in a squirrel cage motor using Discrete Wavelet Transform (DWT)

I. García-Martínez, M. Peña-Cabrera, R. Osorio-Comparán,
I. Lopez-Juarez, O. Molotla, G. Lefranc

Irving García-Martínez
Engineering Faculty, National Autonomous University of Mexico (UNAM)
Circuito Escolar S/N, Ciudad Universitaria, CDMX, México. enrique.bin.v@gmail.com

Mario Peña-Cabrera*
Department of Computer Systems Engineering and Automation
IIMAS, National Autonomous University of Mexico (UNAM)
Circuito Escolar S/N, Ciudad Universitaria, CDMX, México. mario.penia@iimas.unam.mx

Román Osorio-Comparán
Department of Computer Systems Engineering and Automation
IIMAS, National Autonomous University of Mexico (UNAM)
Circuito Escolar S/N, Ciudad Universitaria, CDMX, México. roman@unam.mx

Ismael López-Juárez
Robotics and Advanced Manufacturing, Center for Research and Advanced Studies (CINVESTAV)
Av Ind Metalurgica 1062, P Ind Saltillo-Ramos Arizpe, Coah. México.
Department of Mechatronics, Autonomous University of Yucatan (UADY)
Av. Ind. No Contaminantes S/N, Mérida, Yuc. México.
ismael.lopez@{cinvestav.mx; correo.uady.mx}

Oscar Molotla
Engineering Faculty, National Autonomous University of Mexico (UNAM)
Circuito Escolar S/N, Ciudad Universitaria, CDMX, México. oscar.molotla85@gmail.com

Gastón Lefranc*
Facultad de Ingeniería, Pontificia Universidad Católica de Valparaíso
Avda. Brasil 2950, Valparaíso, Chile. gaston.lefranc@pucv.cl

Abstract

This paper presents a new method for early detection of broken rings and bars in induction motors operating in steady state. The approach uses multispectral analysis based on the Discrete Wavelet Transform (DWT) applied to stator current analysis. A comparison is made between the results obtained using Daubechies wavelets of levels 44 and 45 (db44 and db45). The method focuses on the energetic analysis of the high-level signal decomposition coefficients to detect the presence of left sideband components, which indicate rotor faults. The experimental results demonstrate the effectiveness of the method in distinguishing between healthy and faulty motor conditions, even under light load conditions where conventional techniques often struggle.

Keywords: Fault detection, Discrete Wavelet Transform, Induction motor, Squirrel cage rotor, Motor current signature analysis, Multispectral analysis, Rotor faults

1 Introduction

In the field of signal analysis for fault detection, a variety of monitoring techniques and methods have been employed [2, 16, 21], with recent advancements incorporating AI-based approaches [8], [7]. However, when it comes to current and voltage analysis, the widely recognized Motor Current Signature Analysis (MCSA) [1, 6, 17] stands out as the most commonly used method. Its popularity can be attributed to its non-invasive nature and the simplicity of data collection, making it an effective and accessible choice for fault detection.

By exploring the types of electrical signals used for current analysis in electric motors, a new area of research emerges to find methods and tools that are better suited to today's requirements. So far, several methods have used discrete wavelet transforms, which have demonstrated the ability to work with signals generated from faulty AC induction motors.

A new method based on multispectral analysis using the Discrete Wavelet Transform (DWT) has been developed for the analysis of steady-state stator currents. A comparison has been made between the results obtained using Daubechies wavelets of levels 44 and 45 (db44 and db45). The method focuses on the study of the energy of the coefficients resulting from the decomposition of the high-level signal as a means of detecting the presence of left sideband components. The energy of these coefficients shows a clear increase when the rotor rings or bars have been broken (Figure 1).

Figure 1: Example of a 400 hp induction motor failure due to constant starting and stopping.

Since the beginning of the 20th century, it has been known that the asymmetrical winding of the rotor of an induction motor will produce an interruption of the electric current in a conductor due to the effects of the induction phenomenon and will induce a voltage in the stator winding at a specific frequency, consequently driving a current at that frequency in the stator [6, 17].

The failure of a broken rotor bar produces a torque variation at twice the slip frequency, resulting in a speed variation that is a function of driveshaft inertia.

The slip (s) is the relative difference between the speeds of the stator magnetic flux (synchronous) and the rotor (mechanical), expressed by the following relationship in equation 1.

Failure of a broken rotor bar produces a torque variation at twice the slip frequency, resulting in a speed variation that is a function of the drive shaft inertia. Slip is the relative difference between the stator (synchronous) and rotor (mechanical) magnetic flux velocities, expressed by the following relationship in equation 1 [18, 20]:

$$S = \frac{n_1 - n}{n_1} \tag{1}$$

where n_1 is the synchronous speed and n is the rotor speed.

The current flowing at that frequency in the stator typically causes a decrease in the magnitude of the current component $f(1-2s)$ (left sideband) and the appearance of a new current component at $f(1+2s)$ (right sideband). The magnitude of this new component can be amplified by modulating the third harmonic flow with respect to time in the stator.

The higher the power train inertia, the greater the resistance to torque and speed oscillation at $2sf$ and consequently the smaller the magnitude of the right sideband $(+2sf)$ compared to the left sideband $(-2sf)$ around the fundamental frequency "f". This indicates that faults in the cage or rotor winding produce two sidebands on either side of the fundamental line or frequency as illustrated in Figure 2.

According to [9], the magnitude of the supply frequency component can be 20 to 1000 times greater than the magnitude of the sidebands.

Variations in the electromagnetic field in the air gap generated by a rotor fault create sideband harmonic components in the stator current spectrum. The stator is traversed by a balanced system of three-phase currents which, according to Ferraris' Theorem, establishes a rotating magnetic field with a synchronous speed (ns).

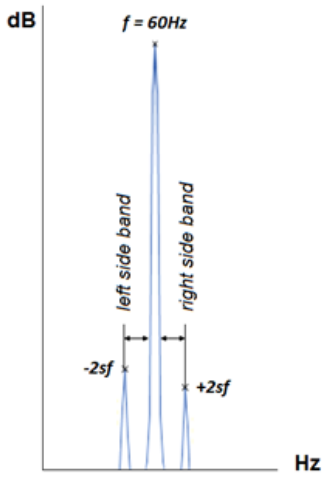

Figure 2: Representation of sidebands and line frequency.

Some Predictive Maintenance has been proposed [12].

This speed is calculated from the linear or fundamental frequency (f_L) of the stator currents and the number of pole pairs (p) using equation 2:

$$n_s = \frac{120 f_1}{p} \tag{2}$$

The rotating field of the stator in squirrel-cage induction motors generates electromotive forces (e.m.f.) in the rotor winding. When this winding is short-circuited, currents appear that generate another magnetic field. The interaction between this field and the synchronous field causes the rotor to move at a speed close to, but always lower than, the synchronous speed. This speed is known as the mechanical speed of the motor (nm). The general expression for this type of machine is given by the equation 3:

$$f_2 = f_1 - \frac{n_m * p}{120} \tag{3}$$

Substituting the expression (2) in (1) we have equation 4.

$$s = \frac{\frac{120 * f_1}{p} - n}{\frac{120 * f_1}{p}} \tag{4}$$

If the reference point of the rotor conducting bars is changed, we can observe the synchronous magnetic field rotating with a relative velocity nr as shown in equation 5:

$$n_r = n_s - n_m = s * n_s \tag{5}$$

Thus, since this magnetic field has p pairs of poles, a rotor conductor bar sees $60nr$ magnetic cycles pass through it in one minute (where one pole pair constitutes one cycle of the magnetic field wave in the air gap). Each magnetic cycle induces one period of the electromotive force time wave as it rotates through a rotor conductor. This causes the rotor phases to induce electromotive forces with a frequency of $60nr$ cycles per minute, or Hz, as shown in Equation 6:

$$f_R = \frac{n_r * p}{120} = s(\frac{\frac{120 * f_L}{p} * p}{120}) \tag{6}$$

Considering equation (2), it can be deduced that the frequency in the rotor phases is given by equation 7:

$$f_R = s * f_L \tag{7}$$

An important advantage of this method, which has been tested in a comparative manner, is that it allows diagnosing the motor condition with less uncertainty under no load and loaded conditions. The faults in these situations are more difficult to distinguish. The experiments were carried out with a squirrel-cage induction motor on a test bench built for diagnostic purposes. A data acquisition system based on an embedded board and an analog-to-digital converter module with programmable gain and high resolution was developed.

2 Continuous wavelets transform

The Continuous Wavelet Transform (CWT) is a signal analysis technique that uses variable-sized windows, allowing for greater precision in time-frequency analysis compared to the Short-Time Fourier Transform (STFT) [13, 15]. In this paper, the CWT is applied to detect faults in induction motors, leveraging its advantages in analyzing non-stationary signals. Smaller regions where high-frequency information is required, as can be seen in the works [3]-[5], [9]-[11], [19] for the detection of failures in induction motors. The idea is shown in Figure 3.

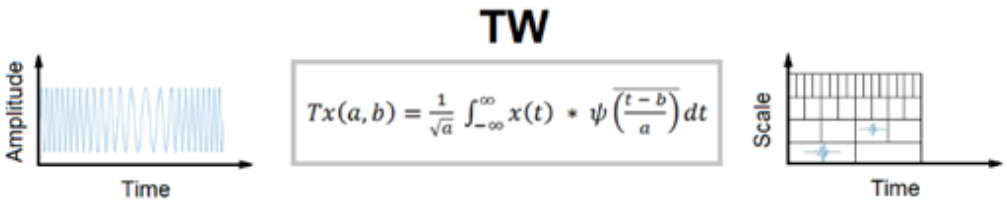

Figure 3: Continuous Wavelet Transform

Key aspects of the application:

1. We use the mother wavelet function $\psi(t)$, which satisfies the finite energy and zero average condition:

$$\int_R \psi = 0 \tag{8}$$

2. The CWT of a continuous signal x(t) is defined by eq. 9:

$$T_x(a,b) = w(a) \int_R x(t)\psi(\frac{t-b}{a})dt \tag{9}$$

Where:
$w(a)$ is a weight function, and generally, $w(a)$ is taken as $1/\sqrt{a}$ to have conservation of energy.
a: scale factor
b: translation factor
ψ_* : complex conjugate of the mother wavelet

3. This transform allows us to analyze the signal at different scales and time positions, which is crucial for detecting specific fault characteristics in motors. Therefore, the wavelet transform is written by eq. 10.

$$T_x(a,b) = \frac{1}{\sqrt{a}} \int_R x(t)\psi(\frac{t-b}{a})dt \tag{10}$$

4. In the analysis, the focus is on scales and positions that correspond to the characteristic frequencies of rotor faults. The normalized wavelet function can be written in a compact form given by equation 11.

$$\psi_{a,b}(t) = \frac{1}{\sqrt{a}}\psi(\frac{t-b}{a}) \tag{11}$$

5. The CWT results are compared with those obtained using traditional Fourier-based methods, evaluating their effectiveness in early failure detection under different loading conditions.

This application of CWT enables more accurate and robust fault detection in induction motors, especially under varying operating conditions or fluctuating loads.

3 Discrete wavelets transform

To apply the Wavelet Transform to a series of numerical data, it is necessary to implement a Discrete Transform [14, 19]. Consider the Wavelet Transform of a continuous signal $x(t)$, but with discrete translation and scaling parameters a and b. A common way to sample the parameters a is by using logarithmic discretization of the scale and linking it to the step size of b, that is, moving in discrete steps to each location of b which is proportional to the scale a. This discretization of the Wavelet has the following equation (12):

$$\psi_{m,n}(t) = \frac{1}{\sqrt{a_0^m}}\psi\left(\frac{t - nb_0a_0^m}{a_0^m}\right) \tag{12}$$

where, $m, n \in Z$ and control the scaling and translation respectively, a_0 is the fixed expansion step size greater than 1, and b_0 is the location parameter that must be greater than zero.

From equation (12), the translation step size $b_0 a_0^m$ is directly proportional to the wavelet scale a_0^m. Therefore, the Wavelet Transform of the continuous signal $x(t)$ using discrete Wavelets of the form (12) is given by equation (13):

$$\psi_{m,n}(t) = \int_{\mathbb{R}} (T_{m,n}x)\, x(t) \frac{1}{a_0^{m/2}} \psi\left(a_0^{-m}t - nb_0\right)\, dt \tag{13}$$

The most common values of a_0 and b_0 are 2 and 1 respectively. The logarithmic scaling in powers of two of the translation and dilation step sizes is known as a dyadic grid array. Substituting $a_0 = 2$ and $b_0 = 1$ in equation (13), the wavelet of the dyadic grid is written as equation (14):

$$\psi_{m,n}(t) = \frac{1}{\sqrt{a_0^m}} \psi\left(\frac{t - nb_0a_0}{a_0^m}\right) \tag{14}$$

Simplifying the expression, it becomes eq. (15):

$$\psi_{m,n}(t) = 2^{-m/2} \psi\left(2^{-m}t - n\right) \tag{15}$$

Discrete Wavelet Transform has an associated dilation equation and its scaling function, which contains information about the smoothness of the signal, as well as having an expression analogous to the wavelet function:

$$\phi_{m,n}(t) = 2^{\frac{-m}{2}} \phi(2^{-m}t - n) \tag{16}$$

which meets

$$\int_R \phi_{0,0}(t)dt = 1 \tag{17}$$

where $\phi_{0,0}(t)$ and is called the scaling function. The scaling function is orthogonal to translations but not to dilations. If the scaling function is convolved with the signal, then we obtain the approximation coefficients. Eq. 18:

$$S_{m,n} = \int_R x(t)\psi_{m,n}(t)dt \tag{18}$$

The approximation coefficients to the m scale are known as the discrete approximation of the signal on that scale. It is possible to generate a continuous approximation of the signal through series according to the form shown in eq. 19:

$$x_m(t) = \sum_{n=-\infty}^{\infty} S_{m,n}\phi_{m,n}(t) \tag{19}$$

where $x_m(t)$ is a smooth version that depends on the signal scaling function $x(t)$ to scale m. It can represent the signal $x(t)$ by an expansion in a combined series of approximation coefficients and detail coefficients as follows, eq. 20:

$$x_m(t) = \sum_{n=-\infty}^{\infty} S_{m,n}\phi_{m,n}(t) + \sum_{m=-\infty}^{m_0} \sum_{n=-\infty}^{\infty} T_{m,n}\psi_{m,n}(t) \tag{20}$$

This original continuous signal equation is decomposed as an approximation of itself, to an arbitrary scale m_0, adding to it a succession of details that are below the m_0 scale. The m-scale detail signal is defined in eq. 21:

$$d_m(t) = \sum_{n=-\infty}^{\infty} T_{m,n}\psi_{m,n}(t) \tag{21}$$

So, equation (21) can be rewritten as eq. (23):

$$x_{(t)} = x_{m_0}(t) + \sum_{n=-\infty}^{\infty d_m(t)} \tag{22}$$

$$x_{m-1}(t) = x_m(t) + d_m(t) \tag{23}$$

That is, if we add the detail signal at an arbitrary scale m to the approximation at equal scale, then we obtain the approximation of the signal at a higher resolution. This process is called multi-resolution rendering.

4 Method and multi-spectral analysis

4.1 First approach: Conventional analysis based on the Discrete Wavelet Transform.

The initial analysis employs the conventional 1-D Discrete Wavelet Transform (DWT) to examine the spectrum of the study signal. After data acquisition, the raw signal is processed using the MATLAB Wavelet Analyzer DWT-1D application to obtain spectra at different levels, also known as multispectral or multiresolution analysis. To identify differences in rotor conditions, the resulting spectrum is used. In addition, the energy of the detail coefficients is calculated, focusing on the level containing the characteristics indicative of the fault condition. Due to the specific nature of this study, this is level four (cD4).

4.2 Second approach: Analysis with new method and Discrete Wavelet transform.

A second analysis is performed using the 1-D Discrete Wavelet Transform, but with prior signal preprocessing. This preprocessing removes signals that may interfere with the analysis and sets a threshold to isolate the signals of interest. (Figure 4).

Figure 4: Data acquisition and processing.

After signal conditioning, multi-resolution or multispectral analysis is applied using the fast wavelet transform algorithm. Several important aspects are considered:

1. Choice of mother wavelet: Two wavelets from the same family but of different levels (Daubechies-44 and Daubechies-45) are used for comparison, considering their correlation with the study signals.
2. Determination of decomposition levels: This is calculated using an expression that varies based on the sampling frequency. Some software tools, like MATLAB, use their own expressions to calculate the decomposition level limit.

The equation (24) chosen to calculate the decomposition levels or branches is:

$$N_{n+1} = \int \left(\frac{\log(\frac{f_s}{f_1})}{\log(2)}\right) + 1 \tag{24}$$

where f_s is the sampling frequency and f_1 is the fundamental frequency.

For this work, with a fundamental frequency of $60Hz$ and a sampling rate of $720Hz$, the calculation yielded 4 levels of decomposition.

It is important to note that the decomposition tree has a decimated dyadic structure, which optimizes the system characteristics by avoiding redundancy in the output data (coefficients). Figure 7 illustrates the four levels of the multilevel decomposition tree, showing the respective outputs of the detail coefficients and the approximation coefficients for level four.

The choice of higher-level mother wavelets (such as db44 and db45) provides more accurate signal details with lower harmonics. At higher levels, the wavelets are less localized in time and oscillate less due to the natural dilation of the wavelet transform, behaving more like ideal filters. While db-45 might work better in theory, correlation with the study signal remains a crucial factor in wavelet selection.

5 Methodologies

The project is divided into four main parts:

1. Preprocessing Validation: In this initial phase, the resulting analyzed signal is compared to the Fourier transform, as it is the most commonly used tool currently for this type of signal analysis. This step serves to validate the effectiveness of our preprocessing technique.
2. Signal Comparison with and without Preprocessing: In this phase, we compare the signals resulting from the analysis with and without our preprocessing method. This comparison helps to evaluate the impact and benefits of the preprocessing step.

3. Multi-Resolution Analysis: We perform an analysis and comparison of the signal using multi-resolution techniques. This approach allows us to examine the signal at different scales and resolutions, potentially revealing features that might be hidden in a single-resolution analysis.
4. Optimization and Fault Detection: In this final phase, we focus on optimizing the signal to the level of interest for comparison. We apply three different criteria and use an appropriate index along with signal energy analysis to determine fault detection. This step aims to improve the accuracy and reliability of our fault detection method.

By structuring the project in this way, we aim to systematically evaluate our proposed method against established techniques, demonstrate the benefits of our preprocessing approach, leverage the advantages of multi-resolution analysis, and ultimately develop a robust fault detection system for the motor under study.

6 Experiment and Tests

The validation of the method was carried out through a series of tests on a 4-pole, 2 Hp squirrel cage induction motor. (Fig. 5). The experimental procedure is as follows:

Figure 5: Healthy rotor, ring and bar failure simulation, broken rotor.

1. Initial Testing: The motor was first tested in its healthy state.
2. Fault Simulation: Failure simulation: After performing healthy state tests, the motor was disassembled to access the rotor. Rotor ring and bar breakages were artificially simulated in the laboratory by carefully removing material to create perforations in the rings and bars. (Fig. 5).
3. Motor Specifications: The motor, a WEG model 00218ET3EM145TCW, was connected in a star configuration with a supply voltage of 220 V. Key specifications include:

   - Nominal voltage: 230 V - Nominal primary current: 5.52 A - Rated power: 2Hp - Number of poles: 4 - Rated speed: 1755rpm - Service factor: 1.25 - Insulation class: F
4. Data Acquisition: Signal data were acquired from Phase 2, selected for its superior stability among the three lines. Primary current measurements were taken during steady state, with samples collected 10 seconds after motor start.
5. Equipment: For data capture, an analog-digital converter was used with a theoretical sampling frequency of 860 samples/s, programmable gain and 16-bit resolution.
6. Analysis: Data acquisition was performed using Python, while Discrete Wavelet Transform (DWT) analysis was performed in MATLAB. A 4-level decomposition using Daubechies-44 and Daubechies-45 mother wavelets was implemented for analysis and comparison.

This comprehensive testing approach allows for a thorough evaluation of the proposed fault detection method under various motor conditions, from a healthy state to simulated faults.

7 Comparative DB-44, DB-45 Methods

The methodology employed in this study used MATLAB as the primary analytical tool. Our approach encompassed several key components:

1. Wavelet transform analysis: We applied wavelet transform techniques to process the motor signals.
2. Multi-resolution analysis: This allowed us to examine the signal at various scales and frequencies.
3. Signal optimization: We refined the signal to improve the detection of fault features.
4. Comparative criteria: Three different criteria were applied and compared to evaluate their effectiveness in fault detection.
5. Energy calculation: We calculated the energy of the signals to apply fault detection indices.
6. Validation: To confirm the results obtained through MATLAB, we performed controlled practical tests using additional tools.

7.1 Analysis and comparison of the signal.

Table 1 presents the bandwidth distribution for each decomposition level, showing both high-frequency (detail) and low-frequency (approximation) signal components. This analysis revealed that our area of interest is mainly concentrated in the fourth level of detail, where signals indicative of motor failures are more prominent.

Table 1: Frequency bands in Hz for TWD with $F_S = 720Hz$

Level	Approximation	Details
1	A1 : [0 , 360]	D1 : [360 , 720]
2	A2 : [0 , 180]	D2 : [180 , 360]
3	A3 : [0 , 90]	D3 : [90 , 195]
4	A4 : [0 , 45]	D4 : [45 , 90]

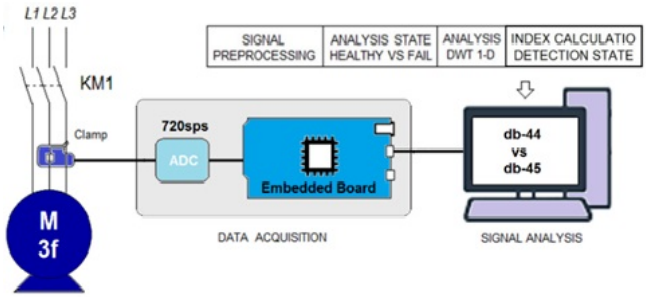

Figure 6: Data acquisition and processing.

This comprehensive approach allows for a robust comparison between Daubechies-44 (DB-44) and Daubechies-45 (DB-45) wavelets, allowing us to assess their relative performance in motor fault detection. The combination of theoretical analysis and practical validation ensures the reliability and applicability of our findings in real-world scenarios.

Figure 7 shows the multi-level decomposition tree. Figure 8 shows the no-load signal analysis for a healthy motor, while Figure 9 shows the same for a motor with a broken bar and ring.

In both cases, variations in the coefficients at the level of interest (cD4) are observed. Although these variations increase with the present fault, they may not definitively indicate an incipient fault, as they could be due to other effects on the motor.

Preprocessed signal analysis: Figure 10 presents the analysis of a preprocessed signal for a healthy motor without load. This preprocessing focuses on detecting early or incipient rotor failures. Compared to the raw signal analysis (figure 11), the preprocessed signal shows smaller variations in the cD4 level, although with a lower amplitude.

The variations increase with current fault, which could indicate a fault at the cD5 level. However, this level does not mean early faults as it is outside the range. The cD4 level shows a higher signal variation, which could suggest a rotor fault, but is not definitive. This behavior could be due to other motor effects.

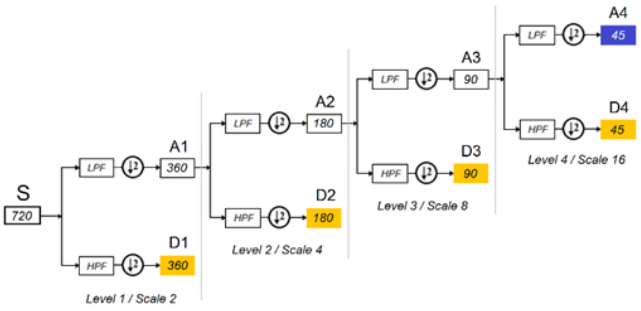

Figure 7: Multilevel decomposition tree

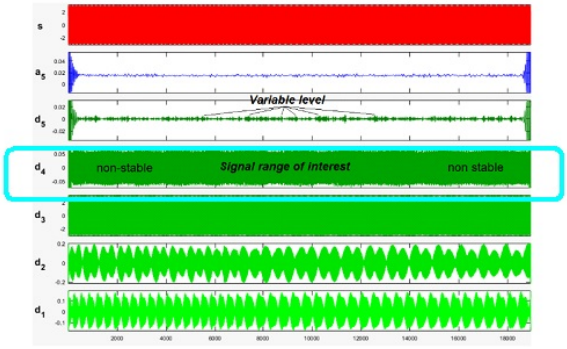

Figure 8: Raw signal healthy empty engine.

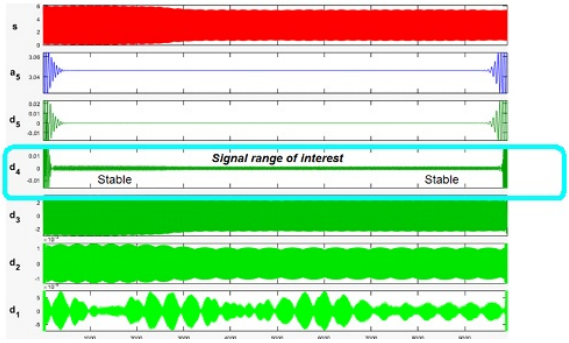

Figure 9: Raw signal fault empty engine.

Figure 10 presents the preprocessed signal to detect early rotor faults in healthy motors. The analysis shows a lower variation in cD4 values compared to the raw signal in figure 8, despite a higher amplitude. This preprocessing is designed to highlight incipient faults, making signal changes more apparent. Stability at cD4 levels is crucial for accurate energy calculations.

Figure 11 shows the analysis of the preprocessed signal for a faulty motor under no-load conditions, maintaining stability at the cD4 level. This consistency is vital for accurate mean calculations and reliable fault diagnoses. Non-uniform data can negatively impact the results, potentially leading to uncertainty or misdiagnosis of the motor's operating state. The accuracy of the method depends on minimizing outliers and signal oscillations.

Signal refinement: Figures 12 and 13 reveal a noticeable difference in coefficient levels at cD4, where rotor fault indicators are located.

Fourteen points from both ends of the signal range have been excluded to improve the results and ensure high-value uniformity. This refinement helps mitigate deviations in coefficient results that could arise from outliers or large magnitude variations.

This refined approach significantly improves the method's ability to detect subtle changes indicative of incipient rotor failure, increasing the overall accuracy and reliability of the diagnostic process. By focusing on

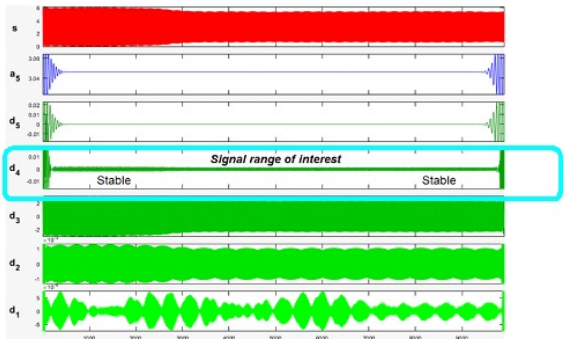

Figure 10: Signal SCPS-1SB healthy empty.

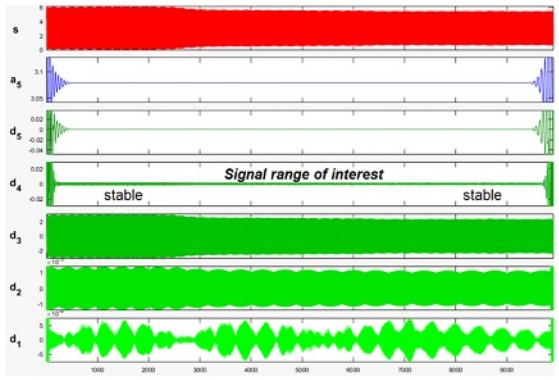

Figure 11: Signal SCPS-1SB fault empty.

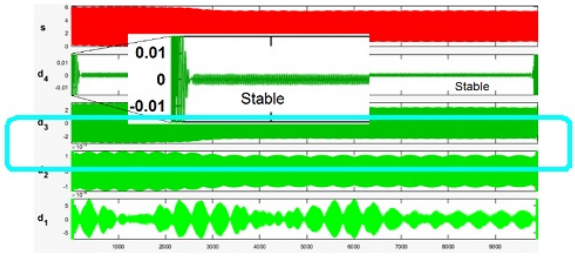

Figure 12: Signal of exit SCPS-1SB empty healthy motor.

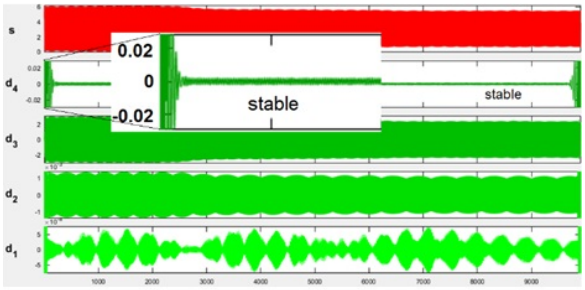

Figure 13: Signal of exit SCPS-1SB empty healthy motor.

the most relevant and stable parts of the signal, we improve the method's sensitivity to early-stage failures while simultaneously reducing the potential for false positives or negatives due to artifacts or signal extremes.

7.2 Applying new method to detect incipient failures.

The new approach to detecting incipient failures in squirrel cage rotor bars and rings focuses on minimizing deviation and eliminating uncertainty caused by subtle differences between motor states. This method improves our ability to detect early stage failures with greater accuracy.

Energy calculation methodology:

The energy of the coefficients is calculated using three different approaches:

1. Energy 1: Calculation using the full range of the level 4 detail signal.
2. Energy 2: Calculation excluding the convolution kernel length from the signal range.
   inenumerate
3. Energy 3: Calculation excluding both the convolution kernel length and 14 additional points, determined through experimental results.

To establish precision and bias metrics, we used a measure of central tendency in all tests, calculating the energy concentrated in each spectrum in the selected range using MATLAB.

Analysis Procedure:

1. Signal conditioning: First, we preprocess the motor signal to improve the fault-related features.
2. Discrete Wavelet Transform: We apply the 1-D Discrete Wavelet Transform to the conditioned signal.
3. Decomposition tree: The signal is then processed through a decomposition tree based on the fast wavelet transform algorithm.
4. Wavelet selection: We use Daubechies-44 (db-44) and Daubechies-45 (db-45) mother wavelets for comparison, considering their correlation with the study signals.
5. Decomposition levels: The number of decomposition levels is determined based on the sampling frequency used.
6. Energy calculation: After signal decomposition, we calculate the energy of the level of interest (cD4), where signals indicative of rotor faults are found (Figure 14).

This comprehensive approach allows us to detect subtle changes in the rotor state, which could indicate the onset of faults before they become more severe. By comparing the results of different wavelet types and energy calculation methods, we can optimize the accuracy and reliability of fault detection.

8 Results

The analysis shows that signals treated with preprocessing present greater stability and less variations compared to those without preprocessing. Furthermore, the results show a clear distinction in magnitudes between the fault-free and faulty states at the level of interest (cD4).

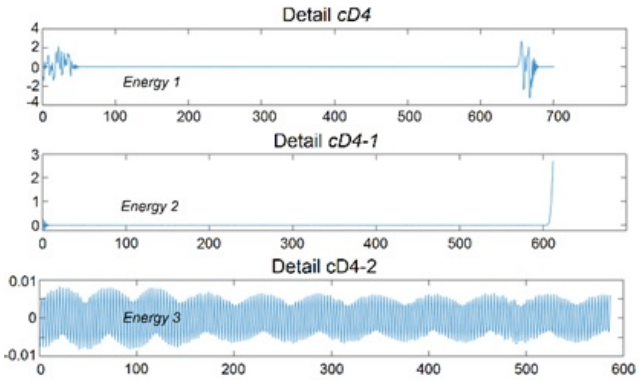

Figure 14: Coefficient signals level 4 (cD4).

8.1 Tests

In the analysis performed at the level of interest for this study (cD4), and when applying the elimination of the signal edges for the different tests performed, among the three ways of performing the signal analysis, a greater stability is presented in the results of energy 3, this characteristic being of great importance to reduce the uncertainty in the detection of incipient faults in the squirrel cage rotor, this can be observed in the results obtained in tables 2 to 5, where the results are shown between the three selected ways of calculating the energy of level 4, as well as when comparing the results obtained between the analysis performed with the mother wavelet DB-44 and DB-45, both the graphs in Figure 12 to 15 indicate greater stability for the calculation of energy when eliminating the kernel length and the extra points, this is confirmed by the average results of the tables that show the lowest level of deviation.

Three different signal analysis methods are applied at the cD4 level, with a particular focus on edge removal. Among them, the Energy 3 calculation method (which excludes both the convolution kernel length and additional points) showed the highest stability. This feature is crucial for reducing uncertainty in the detection of incipient faults in squirrel cage rotors.

Key Findings:

1. Stability Comparison: Tables 2 through 5 present the results of the three energy calculation methods. Energy 3 consistently demonstrated the highest stability across all tests.
2. Wavelet Comparison: We compared the analyses using Daubechies-44 (DB-44) and Daubechies-45 (DB-45) mother wavelets. The results highlight the differences in performance between these two wavelets.
3. Graphical Representation: Figures 15,16 visually confirm the superior stability of the Energy 3 calculation method, which removes the core length and extra points from the signal edges.
4. Statistical Validation: The average results in the tables show the lowest level of deviation for the Energy 3 method, further supporting its effectiveness.

This improved stability and reduced drift in the Energy 3 method significantly improve our ability to detect incipient rotor faults with increased confidence. The clear differentiation between fault-free and faulty states at the cD4 level provides a solid foundation for early fault detection in squirrel-cage induction motors.

These findings underscore the importance of proper signal preprocessing and energy calculation methods to improve the accuracy and reliability of motor fault detection systems.

Tests were performed on an induction motor under various conditions, using Daubechies-44 (db-44) and Daubechies-45 (db-45) wavelets for signal analysis. Our results demonstrate the effectiveness of different energy calculation methods for detecting motor faults.

1. Healhy Motor, No-Load Condition (db-44 Analysis):

Table 2 presents the absolute deviation results for a good engine under no-load conditions, analyzed with db-44. Using a measure of central tendency as a reference, we calculate the average absolute deviations: Energy 1: 40.2%; Energy 2: 61.02%; Energy 3: 11.8%. The Energy 3 method shows the lowest deviation, indicating its superior stability.

2. Faulty Motor (Broken Bar and Ring), No-Load Condition (db-44 Analysis):

Table 3 shows the results for a faulty motor under no-load conditions, analyzed with db-44. Average absolute deviations: Energy 1: 19.2%; Energy 2: 35.8%; Energy 3: 13.09%. Again, the Energy 3 method demonstrates the lowest deviation and maintains its effectiveness regardless of the motor condition.

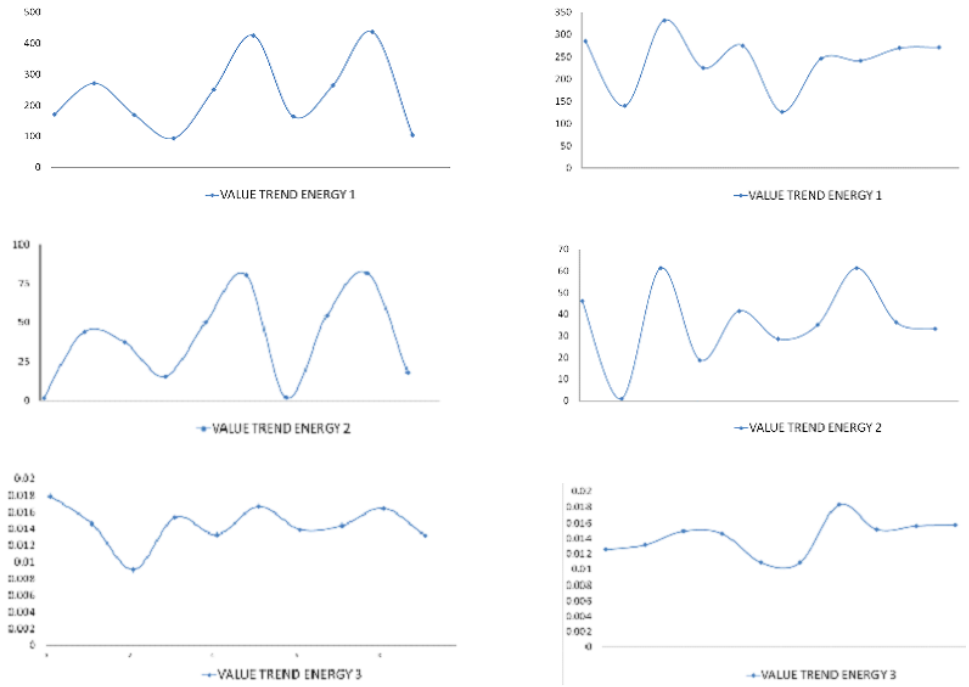

Figure 15: (a)Motor at idle without failure db-44 (b) Motor at idle with failure db-44

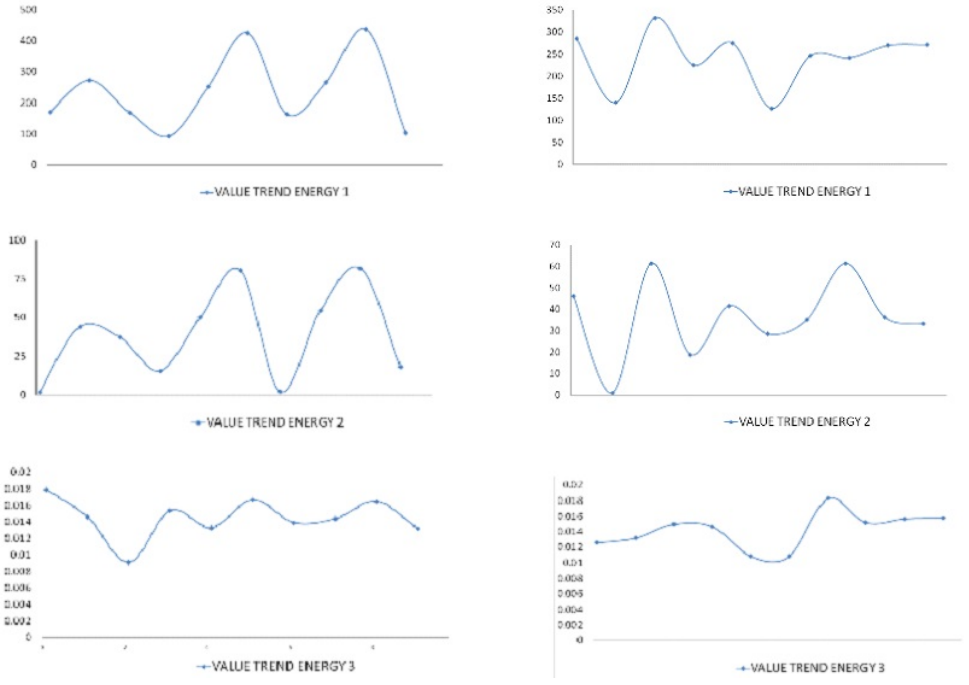

Figure 16: (a)Idle motor signal without failure (b)Idle motor signal with failure db-45

Table 2: Absolute deviation engine in empty non-fault DB-44

Number of Test	Dev. Test Energy 1	Dev. Energy 2	Dev. ABS Energy 3
10	27.0127	95.4137	23.4482
20	15.4113	15.4113	0.6896
30	27.7632	3.30569	37.2413
40	60.0867	59.3823	6.2068
50	6.7053	29.1866	8.2758
60	80.9629	108.2676	15.1724
70	30.3361	94.4955	4.1379
80	12.3141	41.3805	0.6896
90	85.6309	111.7450	13.7931
100	55.8259	52.5289	8.9655

Table 3: Absolute deviation engine in empty fault DB-44

Number of Test	Dev. Test Energy 1	Dev. Energy 2	Dev. ABS Energy 3
10	18.1415	27.0949	11.4546
20	42.1134	97.5832	7.2382
30	37.7641	68.8925	5.4111
40	6.7083	48.1040	3.3028
50	14.0838	14.3827	23.4012
60	47.4215	21.4249	23.4012
70	1.9328	3.5821	28.6015
80	0.0158	68.8579	6.8165
90	11.7936	0.0004	10.3302
100	12.5114	8.5331	11.0330

3. Healthy Motor, No-Load Condition (db-45 Analysis):
Table 4 presents the results for a healthy motor under no-load conditions, analyzed with db-45. Average absolute deviations: Energy 1: 34.8%; Energy 2: 41.7%; Energy 3: 11.8%. The Energy 3 method consistently shows the lowest deviation in the different wavelet analyses.

Table 4: Absolute deviation engine in empty non-fault DB-45

Number of Test	Dev. Test Energy 1	Dev. Energy 2	Dev. ABS Energy 3
10	12.9780	32.9205	23.5023
20	2.3204	9.0224	0.4608
30	31.0811	41.4120	37.3271
40	35.3413	50.8000	6.9124
50	0.5845	4.1685	7.8341
60	87.5784	77.4172	15.2073
70	27.9249	10.6538	4.1474
80	0.4917	32.4465	0.4608
90	85.8663	83.4248	13.3640
100	63.8917	74.9040	9.6774

4. Faulty Motor (Broken Bar and Ring), No-Load Condition (db-45 Analysis):
Table 5 shows results for a faulty motor under no-load conditions, analyzed using db-45. Average absolute deviations: Energy 1: 24.04%; Energy 2: 15.3%; Energy 3: 11.1%

These results consistently demonstrate that the Energy 3 calculation method provides the most stable and reliable results under different motor conditions and wavelet types. This stability is crucial for the accurate detection of incipient faults in squirrel cage rotors, thereby reducing uncertainty in fault diagnosis.

Table 5: Absolute deviation engine in empty fault DB-45 in percentage

Number of Test	Dev. Test Energy 1	Dev. Energy 2	Dev. ABS Energy 3
10	58.1918	51.7871	11.4877
20	24.1447	0.8292	6.7796
30	36.5059	9.7479	5.4613
40	24.9554	4.4233	2.6365
50	1.4057	2.9663	23.7288
60	20.1569	42.6885	22.787
70	8.4249	13.4931	28.0602
80	24.1321	19.5553	7.3446
90	23.3965	0.2140	10.1694
100	19.1571	7.4274	11.1111

8.2 Approach for the new method for the detection of incipient faults.

The new method for fault detection in squirrel cage rotor bars and rings focuses on specific features that allow identifying incipient faults with greater precision, reducing the uncertainty caused by subtle differences between motor states. The analysis employs the 1-D Discrete Wavelet Transform, applying a decomposition tree based on the Fast Wavelet Transform algorithm after signal conditioning. The mother wavelets db-44 and db-45 are used to compare results, considering their correlation with the study signals. The decomposition levels are determined according to the sampling frequency used.

9 Conclusions

This paper presents a new method for detecting faults in squirrel cage rotor bars and rings that focuses on specific features that allow for more accurate identification of incipient faults, reducing the uncertainty caused by subtle differences between motor states. The analysis employs the 1-D Discrete Wavelet Transform, applying a decomposition tree based on the Fast Wavelet Transform algorithm after signal conditioning. The mother wavelets db-44 and db-45 are used to compare results, considering their correlation with the study signals. The decomposition levels are determined according to the sampling frequency used.

After analysis through the decomposition tree, the energy of the level of interest cD4 is calculated, where signals indicative of the presence or absence of rotor faults are found. This approach allows for earlier and more accurate detection of incipient rotor faults.

In today's fast-paced world, predictive and early maintenance have become increasingly crucial, especially for industries that rely on induction motors. This paper presents a new method for early detection of ring and bar breakage in steady-state induction motors. Experiments performed on star-connected squirrel-cage induction motors demonstrate that this method reduces uncertainty in determining the rotor state and provides greater stability regardless of the rotor state or the mother wavelet used, thus increasing certainty in identifying incipient faults.

The method is based on proper signal conditioning and the application of a special filter. This filter has two purposes: to remove the line or fundamental frequency and to perform anti-aliasing. It is designed based on widely studied frequencies known to indicate rotor damage. This filter, combined with signal acquisition elements, forms the single-sideband signal conditioning preprocessing system (SCPS-1SB).

The process continues with the calculation of levels of the decomposition tree for multi-resolution analysis based on the discrete wavelet transform. In this case, four levels are used, with special attention to the detail coefficients of the fourth level. These coefficients are post-processed, including energy calculation using an appropriate index and removal of extreme coefficients. This optimization reduces the core length to 14 points, resulting in lower deviations compared to analyses without SCPS-1SB.

The results indicate that the proposed signal preprocessing method produces more stable and consistent results compared to analysis without preprocessing. The "Energy 3" calculation method, which removes edge coefficients and optimizes the core length, shows the lowest deviation and highest stability, clearly differentiating between healthy and faulty motor conditions.

This method significantly reduces uncertainty and improves detection of incipient faults in broken rings and cranks compared to conventional DWT analysis. It performs consistently regardless of the original wavelet used, although conventional DWT analysis shows notable differences between db-44 and db-45 wavelets. The proposed approach can more clearly diagnose various conditions, even under light load conditions where state distinction is often challenging. By focusing on the frequencies of interest and refining the signal characteristics, this method increases the accuracy in squirrel cage rotor fault detection and diagnosis.

Acknowledgements

The authors would like to acknowledge the financial support provided by the National Autonomous University of Mexico (UNAM) through the PAPIIT Project No. IN104424 directed by Dr. Helena Montserrat Gómez Adorno.

References

[1] Antonino-Daviu J., Quijano López A., Rubbiolo M., Climente-Alarcon V., (2017) Diagnosis of the rotor condition in electric motors operating in mining facilities through the analysis of motor currents, IEEE Industry Applications Society Annual Meeting

[2] Castelli M. J., Fossati J.P., Andrade (2008)," Metodología de monitoreo, detection de fallos y diagnostico en motores asíncronos", IEEE, 7º encuentro de Energía, Potencia M. T., Instrumentación y Medidas, pp. 91-97.

[3] Ciprian H., Loránd S.(2011), "Wavelet Analysis and Park's Vector Based Condition Monitoring of Induction Machines", Journal of ComputerScience and Control Systems, Vol. 5, No. 2, pp. 35-38

[4] Cusidó, Romeral L., Ortega J. A., Rosero J. A., García Espinosa A. (2008), "Fault Detection in Induction Machines Using J. Power Spectral Density in Wavelet Decomposition", IEEE Transactions on industrial electronics, Vol. 55, No. 2, pp. 633-643.ons Society Annual Meeting.

[5] Espinosa Pérez D., Delgado J., (2012). Wavelets y Superresolución. Master These. Universidad Autónoma Metropolitana Unidad Iztapalapa

[6] Fernández Tavitas D. A., Nieto González J. P. (2014), "Detección de barras rotas en motores de inducción utilizando SMCSA (Square Motor Current Signature Analysis)", Research in Computing Science, Vol.73, pp. 193–202.

[7] Guojian Li, Jian Wang, Yingwu Qin, Xuefeng Bai, Yuhan Jiang, Yi Deng, Zhiyuan Ma, Mengnan Cao. Enhancing Wind Farm Reliability: A Field of View Enhanced Convolutional Neural Network-Based Model for Fault Diagnosis and Prevention. International Journal of Computers Communications & Control. Vol. 19 No. 3 (2024). https://doi.org/10.15837/ijccc.2024.3.6609.

[8] Liu, J.Z.; Qu, Q.L. ; Yang, H.Y. ; Zhang, J.M., Liu, Z.D. Deep Learning-based Intelligent Fault Diagnosis for Power Distribution Networks. INTERNATIONAL JOURNAL OF COMPUTERS COMMUNICATIONS & CONTROL. Vol 19, Issue 4. AUG 2024. DOI10.15837/ijccc.2024.4.6607

[9] Martínez García Irving I and Peña Cabrera J. Mario, Analysis Optimization and Comparison to Detect Failures in the Squirrel-Cage Rotor using High-Level Wavelets, International Journal of Electrical and Electronics Research (IJEER) , Volume 11, Issue 4, Pages 966-972, e-ISSN: 2347-470X

[10] Moin Siddiqui K., Giri V.K, (2012) "Broken Rotor Bar Fault Detection in Induction Motors Using Wavelet Transform", International Conference on Computing, Electronics and Electrical Technologies [ICCEET], pp. 1-6.

[11] Navarro Fuentes J., Elizarraras Martinez D. (2010), Introducción a la transformada Wavelet Continua. Editorial Reverté.

[12] Pătras,cu, A.; Bucur, C.; Tănăsescu, A.; Toader F.A. (2024). Proposal of a Machine Learning Predictive Maintenance Solution Architecture, International Journal of Computers Communications & Control, 19(3), 6499, 2024. https://doi.org/10.15837/ijccc.2024.3.6499

[13] Pineda caballero A. R. (1998). Teoría de Wavelets, una alternative, Thesis, Universidad Nacional Autonoma de Mexico, Acatlan, México.

[14] Pu Shi, Zheng Chen, Yuriy Vagapov. Wavelet Transform based Broken Rotor-bar Fault Detection and Diagnosis Performance Evaluations. International Journal of Computer Applications. 69, 14 (May 2013), 36-43. DOI=10.5120/11913-8033.

[15] Quian Tao, Vai Mang, Xu yuesheng, (2007). Wavelet Analysis and Applications. Basilea Suiza: Birkhäuser Verlag..

[16] Rezazadeh M., Mariun N., Hamiruce M., Misron N. (2011), "Rotor fault condition monitoring techniques for squirrel-cage induction machine: A review", Mechanical Systems and Signal Processing, Vol. 5. No. 8, pp.2827-2848.

[17] Sbaa S, Bessous N, Pusca R, Romary R (2020). A comparative study dedicated to rotor failure detection in induction motors using MCSA, DWT, and EMD techniques. 2020 International Conference on Electrical Engineering (ICEE)DOI: 10.1109/ICEE49691.2020.9249774, https://univ-artois.hal.science/hal-04296850/document.

[18] Singh M. , Gafoor Shaik A. , "Broken Rotor Bar Fault Diagnosis of a Three-phase Induction Motor using Discrete Wavelet Transform"(2019), IEEE PES GTD Grand International Conference and Exposition Asia (GTD Asia), pp. 13-17, 2019.

[19] Viraj U. Patel (2019), "Condition Monitoring of Induction Motor for Broken Rotor Bar using Discrete Wavelet Transform and K-nearest Neighbor", International Conference on Computing Methodologies and Communication (ICCMC).

[20] Yun Guo C., Ping Li J. (2013), "Development and future of wavelet analysis", 10th International Computer Conference on Wavelet Active Media Technology and Information Processing (ICCWAMTIP), pp. 335-338,.https://doi.org/10.15837/ijccc.2024.1.4xyz

[21] Zhang, C.M.; Xu, X.Q.; Liu, S.L.; Li, Y.J.; Jiang, J.F. (2024). Fault Diagnosis and Localization of Transmission Lines Based on R-Net Algorithm Optimized by Feature Pyramid Network, International Journal of Computers Communications & Control, 19(4), 6608, 2024. https://doi.org/10.15837/ijccc.2024.4.6608

Cite this paper as:
García-Martínez I., Peña-Cabrera M., Osorio-Comparán R., Lopez-Juarez, I., Molotla, O., Lefranc G. (2025).Theoretical approach and implementation using discrete wavelet transform for early fault detection in squirrel cage motor current, *International Journal of Computers Communications & Control*, 20(3), 6919, 2025.
https://doi.org/10.15837/ijccc.2025.3.6919